Multiphoton fluorescence lifetime contrast in deep tissue imaging: prospects in redox imaging and disease diagnosis

V. Krishnan Ramanujan
Jian-Hua Zhang
Eva Biener
Brian Herman
University of Texas Health Science Center at San Antonio
Department of Cellular and Structural Biology
7703 Floyd Curl Drive
San Antonio, Texas 78229
E-mail: krsna@uthscsa.edu

Abstract. Turbid tissues pose serious problems of strong absorption and scattering that make steady state fluorescence imaging methods less successful in imaging tissue layers deeper than a few tens of micrometers. Complications arise as one progresses from imaging cells to tissues to whole animal—which include enormous autofluorescence background in tissues and poor signal from regions of interest. Since the steady state, intensity-based methods cannot discriminate the photons arising from the fluorophores and the autofluorescence background, it is almost impractical to isolate these two signals. We describe multiphoton fluorescence lifetime imaging methods in the time domain to demonstrate fluorescence lifetime contrast in discriminating autofluorescence background from the fluorescent signals. Since the photophysical schemes of the fluorophore and autofluorescence contributions are distinct, it is feasible to isolate these two contributions in every pixel based only on their decay constants without compromising the SNR. We present preliminary lifetime measurements to characterize autofluorescence in various cell lines and *ex vivo* tissues obtained from mouse models. Together, these results suggest a novel direction in obtaining quantitative information from endogenous tissue fluorescence without any exogenous staining. The prospects for this approach in metabolic redox imaging and disease diagnosis are discussed.
[DOI: 10.1117/1.2098753]

Keywords: fluorescence lifetime imaging; multiphoton microscopy; autofluorescence; tissue imaging; redox imaging.

Paper SS04253R received Dec. 17, 2004; revised manuscript received Mar. 28, 2005; accepted for publication Apr. 5, 2005; published online Oct. 21, 2005.

1 Introduction

Traditional methodologies for investigating the interaction of light with biological tissues were limited to spectroscopic measurements that exploited changes in linear absorption coefficients to interpret biochemical signals from pathological specimens.[1] Recently, there has been an upsurge in fluorescence imaging modalities in disease diagnosis owing to their superior sensitivity and specificity.[2] Besides monitoring the molecular biochemistry within living cells, it has also become possible to visualize physiological processes in higher cellular organization networks such as tissues and organs. One of the major advantages of optical imaging modalities in disease diagnosis (e.g., detection of benign/malignant tumor) is that it is nonionizing as compared with conventional x-ray mammography and positron emission tomography, which requires injection of radioactive tracers inside the organs. Existing noninvasive optical imaging modalities such as optical coherence tomography (OCT) and near-infrared (NIR) diffuse optical tomography can provide sensitive information from turbid tissues based on their differences in absorption characteristics.[3,4] These methods have been successfully applied to obtain information on tissue hemoglobin concentration and oxygen saturation. Problems associated with optimizing NIR image reconstruction lead to lesser reliability in contrast for objects smaller[5] than 8 mm. This limitation can be serious if one wishes to employ these techniques in early diagnosis of cancerous lesions, which can escape detection because of their much smaller size than the minimum detectable level by diffuse optical tomography methods. On the other hand, fluorescence imaging systems possess (1) greater flexibility in design and implementation, (2) higher spatial resolution and specificity for smaller objects, and finally (3) possibilities to obtain and analyze results—leading to direct visualization of physiological processes in real time. Wide-field fluorescence microscopy and laser scanning confocal microscopy methods have been successfully employed to understand a variety of phenomena in fixed or living cells in the UV to far-IR optical window.[6,7] However, turbid tissues pose serious problems of strong absorption and enormous scattering that make these

Address all correspondence to V. Krishnan Ramanujan, Cellular and Structural Biology, University of Texas Health Science Center, 7703 Floyd Curl Drive, San Antonio, TX 78229. Tel.: (210) 567-4571; Fax: (210) 567-3803; E-mail: krsna@uthscsa.edu

1083-3668/2005/10(5)/051407/11/$22.00 © 2005 SPIE

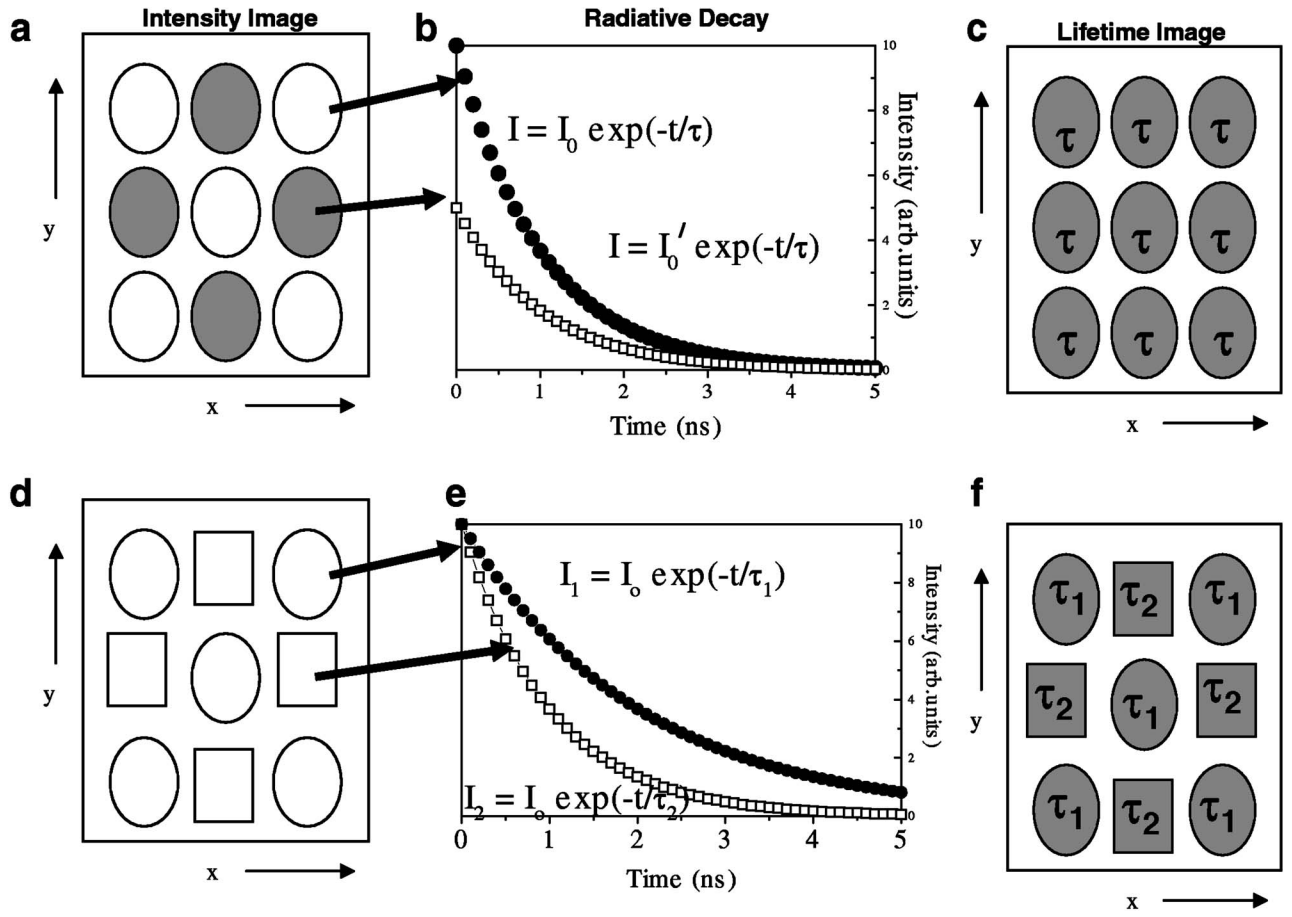

Fig. 1 Defining lifetime contrast in imaging paradigm: (a) 2-D field of view showing spatial variation of intensity (concentration) of a fluorophore (circle) in every pixel. Since the radiative decay constant (τ) is the same for the fluorophore independent of concentration (b), the calculated lifetime image (c) shows a uniform distribution of lifetime values. (d) Intensity image showing two spectrally similar fluorophores (square and circle) having the same intensity (concentration). If the radiative decays for these fluorophores are different (τ_1 and τ_2), as shown in (e), then they can be distinguished in the lifetime image (f) despite their spectral similarity.

fluorescence imaging methods less successful in imaging tissue layers deeper than a few tens of micrometers. In this context, multiphoton excitation methods have proved more suitable in providing clear images even from deeper tissue layers, owing to their NIR excitation wavelengths (700 to 1000 nm) and hence reduced absorption of the excitation light.[8] Complications arise as one progresses from imaging cells to tissues to a whole animal: first is poor signal from regions of interest deep in the tissues, and second is enormous autofluorescence background of the surrounding tissue layers. Together, these two factors decrease SNR in the final images. An endogeneous autofluorescence background has a fairly wide emission band encompassing the wavelength range 450 to 700 nm and is convolved in every pixel of the image with varying amplitudes. Since the steady state, intensity-based methods cannot discriminate the photons arising from the fluorophores and the autofluorescence background, it is almost impossible to isolate these two signals. This problem brings up the necessity to identify an intrinsic parameter that can discriminate fluorescent signals from the surrounding autofluorescence background based on their intrinsic photophysical characteristics rather than external factors such as filters. Since the photophysical schemes of the fluorophore and autofluorescence contributions are distinct, fluorescence lifetime (τ) therefore can be employed as an "intrinsic contrast" parameter in obtaining information from cells and tissues without compromising the SNR. In this paper, we describe multiphoton fluorescence lifetime imaging methods in the time domain to demonstrate lifetime contrast in discriminating autofluorescence background from the fluorescent signals. Figure 1 defines the concept of lifetime contrast in imaging. To demonstrate the feasibility of autofluorescence discrimination by lifetime imaging in cells/tissues, we present some preliminary lifetime data obtained in various cell lines and *ex vivo* tissues obtained from mouse models. Together, these results suggest a novel direction in obtaining quantitative information from endogenous tissue fluorescence without any exogenous staining. The prospects for this approach in disease diagnosis are discussed.

2 Materials and Methods

2.1 *Multiphoton Fluorescence Lifetime Imaging in the Time Domain*

Fluorescence lifetime imaging microscopy (FLIM) methods currently available can be broadly classified into two groups,

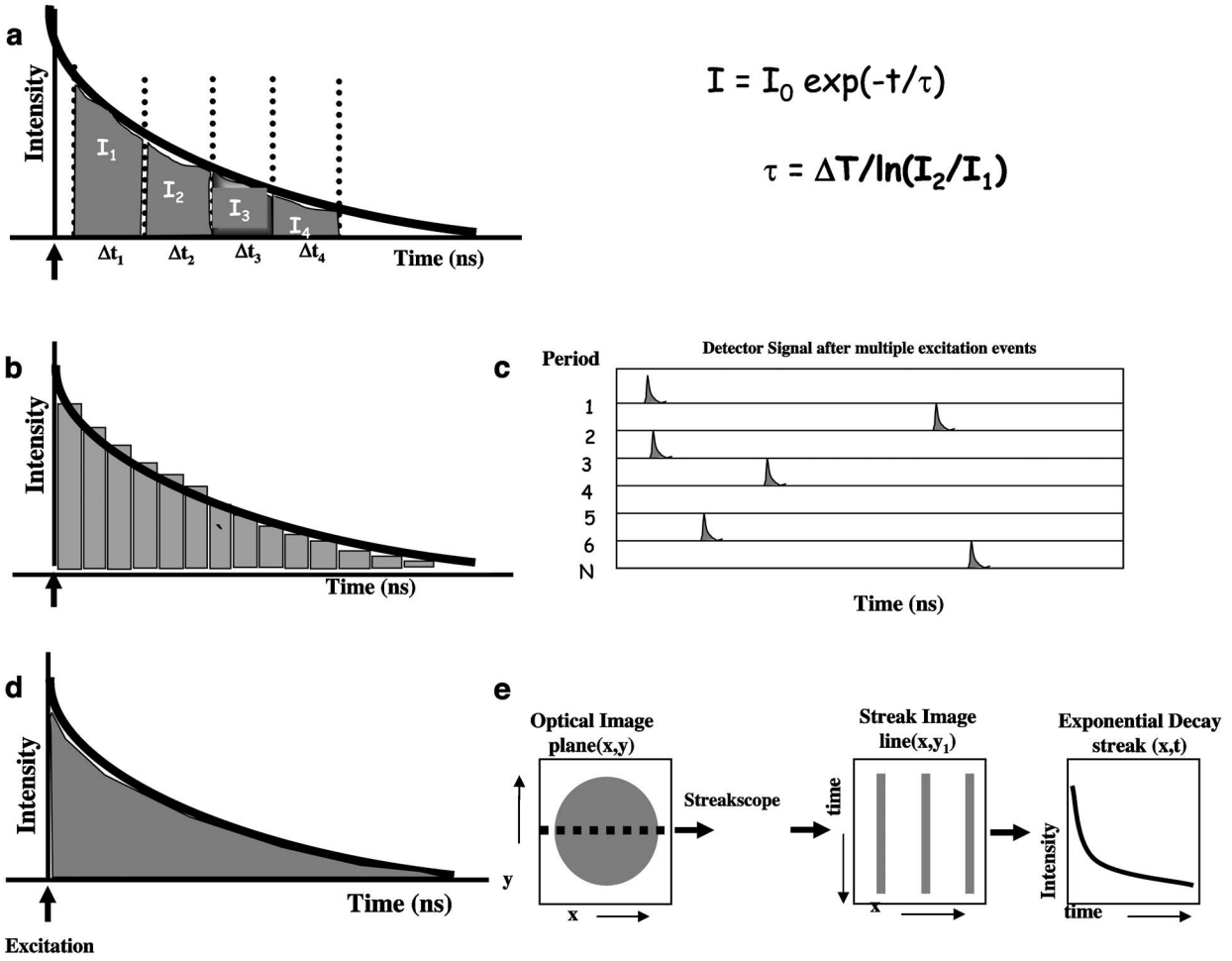

Fig. 2 Schematics of time-domain fluorescence lifetime imaging microscopy. (a) Multigate detection method showing four time windows with a typical gate width of ~2 ns each. The specimen is excited with femtosecond laser pulses and the fluorescence intensity decay curve is sampled by sequentially opening the time windows and by collecting the integrated intensities ($I_1, I_2, \ldots$). Lifetime τ is computed by ratiometry. (b) In the time-correlated single-photon counting method, following multiphoton excitation of the specimen, individual photons are detected. By sorting the collected photons based on the time elapsed between the excitation pulse and their detection time into individual time bins (width ~20 ps) by fast electronics, a photon histogram is built based on the individually counted photons, as shown in (c). Lifetime is then calculated by fitting the profile of this histogram. (d) In the StreakFLIM method, the streak camera detects the entire fluorescence decay (time resolution ~15 ps) without any time gating or prolonged exposure to build the photon histogram. The lifetime is calculated by fitting the decay curve at each pixel. The sequence of events in data acquisition is schematically depicted in (e).

namely, (1) time-domain and (2) frequency-domain FLIM. For a detailed discussion of these methods and a comparative survey of relative merits/demerits of these methods, see an earlier review article.[9] Briefly, in the case of time-domain methods, the specimen is illuminated with pulsed light and the subsequent fluorescence emission decay is recorded by fast detectors. By fitting the observed emission decay to an appropriate mathematical model, the fluorescence lifetimes of the different fluorescent species within the specimen are extracted. Regardless of the method adopted, either single-photon or multiphoton excitation can be used to measure lifetimes. In this article, we limit our discussion only to time-domain FLIM systems employing multiphoton excitation.

The most explored method in measuring lifetime in a scanning microscope is by employing time-gated detection pioneered by Sytsma et al.[10] and Gerritsen et al.[11] The principle of detection is based on sampling fluorescence intensity decay curve with two or more time gates (typical width=2 ns), which can be opened sequentially after every laser pulse. Figure 2(a) shows a schematic of the detection with four time gates. This system has proved capable of high photon efficiency and high maximum count rate capability in measuring rapid lifetime determination in living cells. It has also been found that the overall performance of multigate detection FLIM system is dominated by the transition-time spread (TTS) characteristics of the photomultiplier tube detector.

Another approach that is particularly suitable in low-light applications is time-correlated single-photon counting[12] (TCSPC). The principle of this method involves detection of single photons of a periodic light signal, the measurement of their detection times and constructing a histogram of the detection times of the single emitted photons from these individual time measurements. Figure 2(b) demonstrates the principle of TCSPC approach. Photon-counting detectors are well suited for low-light-level detection as well as for providing quantized pulses for every photon event.[13,14] This makes the

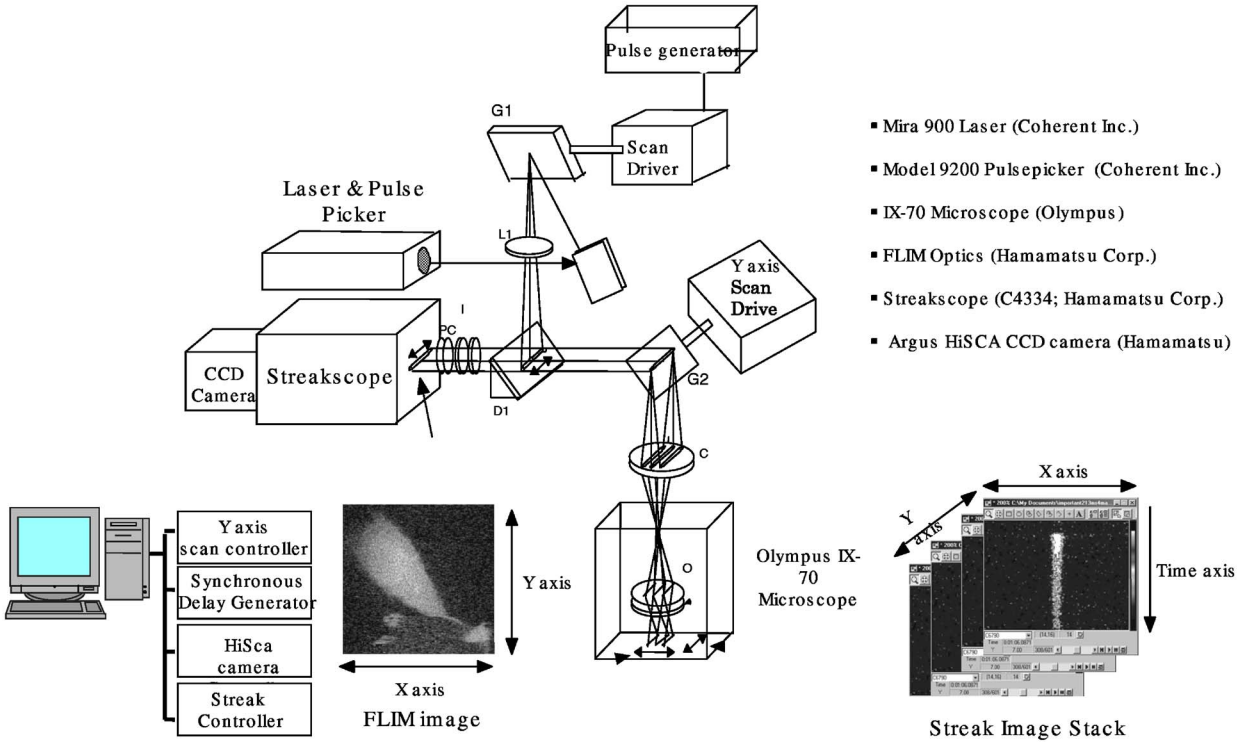

Fig. 3 Optical layout of StreakFLIM system: G1, horizontal galvanometer mirror; G2, vertical galvanometer mirror; L1, focusing relay lens; C, coupling lens for sideport optics; I, imaging lens; O, microscope objective lens; D1, dichroic mirror; and PC, photocathode.

measurement of lifetimes more accurate, although the detectors suffer from poor dynamic range as compared to their area detector counterparts. The maximum count rates detectable by the microchannel plate photon detectors in TCSPC are limited to 10^6 photons/s, which limits the dynamic range in this approach. Improved fast detectors, compatibility with laser scanning microscope modules, and advanced data analysis algorithms have made TCSPC FLIM systems a reliable option. Furthermore, in low-light situations, the histogram approach used in TCSPC systems can lead to significantly longer data acquisition times, thereby making live-cell FLIM imaging difficult.

2.2 *Multiphoton FLIM Using a Streak Camera*

Our group recently developed a novel multiphoton FLIM system using a streak camera[15,16] (StreakFLIM). An important feature of this system is that the entire decay in every pixel is collected without any time gating or prolonged excitation to build photon count histogram. The lifetime parameter can be extracted in each pixel by fitting to the intensity decay in every pixel. Figure 2(c) demonstrates the principle of operation of StreakFLIM system, and Fig. 3 provides the optical schematic of the system. A more detailed technical description of the system can be found in earlier publications.[15,16] Briefly, the heart of the StreakFLIM system is the streak camera (or streakscope), a device that can measure ultrafast light phenomena with a temporal resolution[17] as low as 2 ps. The streak camera consists of a photocathode surface, a pair of sweep electrodes, a microchannel plate (MCP) to amplify photoelectrons coming off the photocathode, and a phosphor screen to detect the amplified output of MCP. Individual optical pulses (fluorescence emission) are collected from every point along a single line as the beam scanner scans across the x axis. When these optical pulses (originating at different points in space and time) strike the photocathode surface, photoelectrons are emitted. As the photoelectrons pass between the pair of sweep electrodes, a high voltage, synchronized with the excitation pulse, is applied to these sweep electrodes. This sweep voltage steers the electron paths away from the horizontal direction at different angles, depending on their arrival time at the electrodes. The photoelectrons then get amplified in MCP and reach the phosphor screen, forming an image of optical pulses arranged in the vertical direction according to the time of their arrival at the sweep electrodes. The earliest pulse is arranged in the uppermost position and the latest pulse is in the bottom-most portion of the phosphor image. The resulting streak image has space as the x axis and time as the y axis. Besides intensity and time information, the streakscope can be used to obtain either spatial or wavelength information. The higher time resolution of the streakscope (Model C4334: 15 ps, Hamamatsu Photonics, Japan) as compared with the fast photomultiplier tube (PMT) (~250 ps)/microchannel plate (~50 ps) makes this system ideal for measuring very short lifetimes reliably well. Figure 2(c) demonstrates the principle of operation of Streak-FLIM.

2.3 *Cells, Tissues, and Microscopy*

HEK 293T and HeLa cells were obtained from the American Type Culture Collection (ATCC). HEK 293T cells were cultured in Dulbecco's modified eagle medium (DMEM) containing 10% fetal bovine serum on poly-d-lysine (Sigma, St. Louis, Missouri) coated coverglasses (Nalge Nunc Interna-

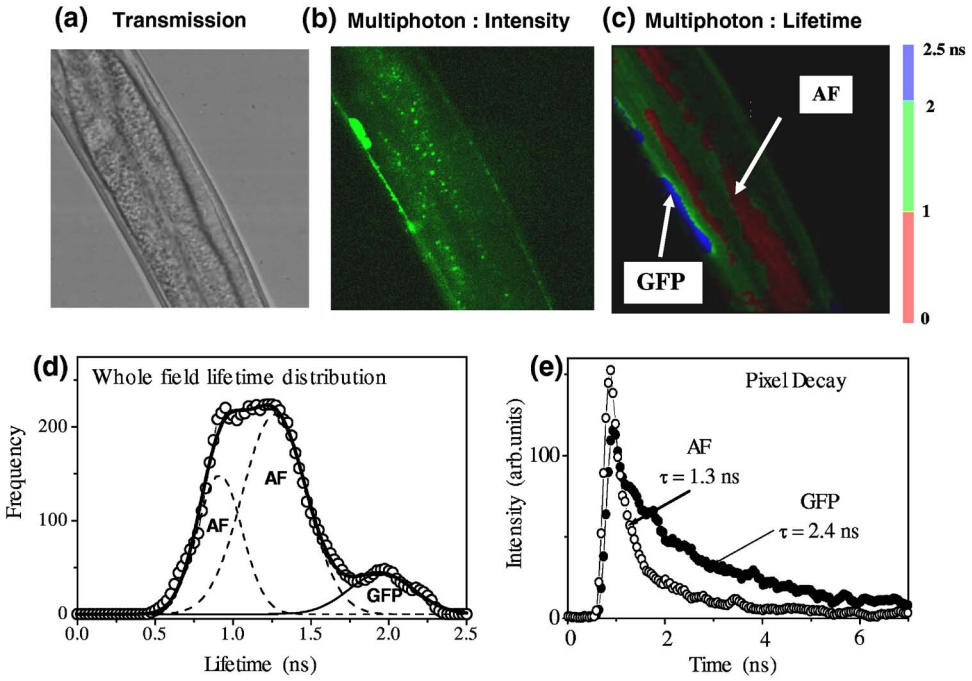

Fig. 4 Autofluorescence discrimination in *C. elegans*. (a) to (c) Transmission, multiphoton intensity, and lifetime images obtained from a live nematode worm (*C. elegans*). The specimen was excited at 850 nm and fluorescence emission was collected with a short-pass filter (SP640 nm). Lifetime images were obtained with the commercial TCSPC module coupled to a Zeiss 510 microscope. A lifetime histogram of the whole field of view (d) shows two distinct autofluorescence peaks and one peak corresponding to green fluorescent protein. (e) Intensity decay at individual pixels marked in (c), showing distinct decays for GFP and autofluorescence.

tional, Napervile, Illinois). HeLa cells were cultured in minimum essential medium (MEM), supplemented with 2 mM/L of L-glutamine and 10% of fetal calf serum. Primary hepatocytes were isolated from C57BL/6 mice by perfusing the liver, as described in Ref. 18. Mice were obtained from the National Institute of Aging. Mice were anesthetized with Ketamine/S.A. Rompun cocktail and liver was perfused through the hepatic portal vein with 0.5-mM EGTA in Ca^{2+}-free Earle's balanced salt solution (EBSS) for 5 min, followed sequentially by wash buffer (0.5% bovine serum albumin and 1.8-mM $CaCl_2$ in Ca^{2+}-free EBSS) and by collagenase buffer (0.06% collagenase, 0.5% bovine serum albumin, and 5-mM $CaCl_2$ in Ca^{2+}-free EBSS) for 10 to 15 min. The liver was then further perfused with wash buffer for 5 min and hepatocytes were collected. After washing three times with cold wash buffer, the hepatocytes were cultured in William's E media supplemented with 5% fetal bovine serum (FBS), 4 μg/ml insulin, 1000 unit/ml penicillin G sodium, 100 μg/ml streptomycin sulfate, and 250 ng/ml amphotericin B in collagen coated chambered cover glasses. All cell lines were maintained at 37°C in an atmosphere of 5% of CO_2 and 95% air. Tissue samples were collected from anesthetized C57BL/6 mice. Freshly collected tissues (skin, heart, kidney) were cut to pieces (~6 to 8 mm thickness) and placed between two coverslips separated by parafilm filling for obtaining optically flat specimens. Tissue specimens were used immediately for microscopy. Nematode worms (*Caenorhabditis elegans*) expressing green fluorescent protein in neurons were maintained in an imaging chamber supplemented with nutrient buffer and 5-mM sodium azide. StreakFLIM or TCSPC FLIM systems were employed to obtain autofluorescence images from cells and tissue specimens. Both these systems are equipped with a Ti:sapphire laser (Coherent Inc., California) for multiphoton excitation and dedicated scanning systems. Data acquisition/analysis was performed by AquaCosmos software (StreakFLIM; Hamamatsu Photonics, Japan) and SPCM/SPC Image software (TCSPC FLIM; Becker & Hickl, Berlin, Germany). Multicomponent analyses were performed by profile fitting in TCSPC FLIM system and by a global analysis module in StreakFLIM system.

3 Results and Discussion

3.1 *Autofluorescence Discrimination in C. elegans*

Green fluorescent protein (GFP) and its various mutants have been extensively used in recent times for monitoring a variety of cellular processes in fixed and living cells.[19,20] In most circumstances, these proteins are overexpressed in cells so that the weak autofluorescence contributions can be ignored as "noise," or suitably subtracted prior to quantification while imaging cells. However, in the case of tissues the comparable intensities of autofluorescence and the signal from fluorescent proteins make the quantification less straightforward. Figure 4 shows a section of a live nematode worm (*C. elegans*) expressing GFP in neurons. The multiphoton intensity image shows neuronal GFP with a bright ganglion. One can also see autofluorescence granules with similar intensities in the gut of the worm. This intestinal autofluorescence can be artifactually interpreted as the leakage of GFP inside the lumen if one compares only the intensity. On the other hand, the lifetime image unequivocally discriminates the neuronal GFP from the surrounding autofluorescence based on the lifetime decay

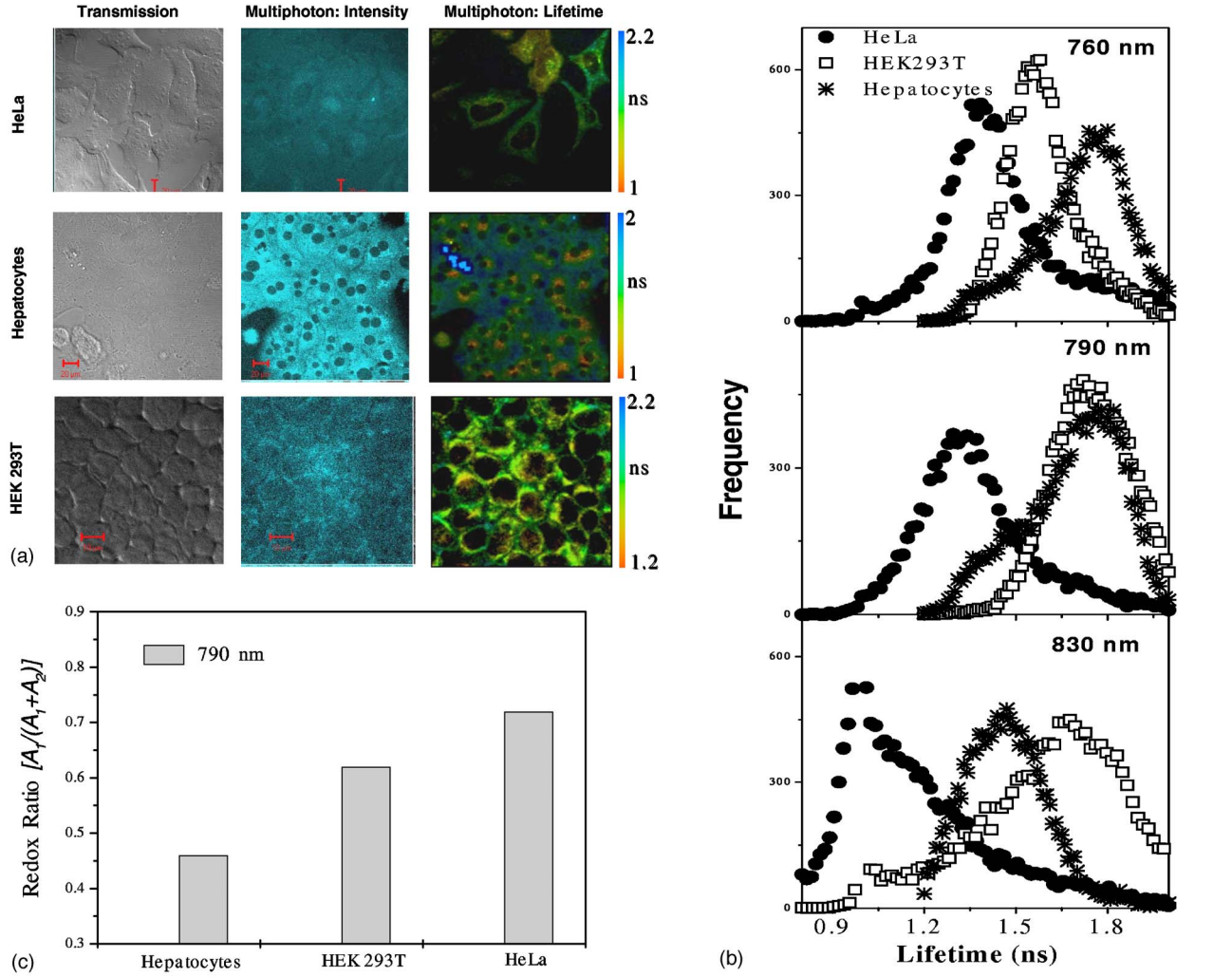

Fig. 5 Representative intensity and lifetime images obtained in live cells in culture for (a) transmission, multiphoton fluorescence intensity, and fluorescence lifetime images obtained from HEK293T epithelial cell line, HeLa cancer cell line, and primary cultures of mouse hepatocytes excited at 790 nm and (b) lifetime histograms obtained from these cells assuming a single-component lifetime analysis and with multiple excitation wavelengths (750, 790, and 830 nm). (c) Redox ratio calculated from the amplitudes of two lifetime components given in Table 2.

curves which are shown in the accompanying graphs [Figs. 4(d) and 4(e)]. The whole-field histogram can be deconvolved to give two peaks corresponding to autofluorescence and one peak corresponding to GFP. Individual pixels selected each at GFP and autofluorescence region (lumen) show distinct decay characteristics with a high contrast. Beyond cuvette measurements, many studies attempted to measure autofluorescence in cells and tissues using imaging modalities where the primary limitation was found to be the excitation sources/filters in UV region (most of autofluorescence gets excited between 270 and 450 nm) and poor microscope optics causing aberrations in UV region. In addition to imaging in cells, fluorescent probes are now designed for staining tissues, and more recently, tumor cells expressing bright fluorescent proteins are implanted inside mouse models to monitor, for example, the progression of tumor and metastasis within the animal.[21] All these methods have been primarily limited to wide-field, filter-based, single-photon excitation approaches. Furthermore, these imaging modalities were being employed more as a visualization tool rather than for precise quantification. The major hurdle in quantitative imaging of fluorescence in tissues is the huge autofluorescence background that reduces the signal-to-background enormously. As can be seen from Fig. 4, fluorescence lifetime contrast can provide a better reliability in quantification of fluorescent regions despite a large autofluorescence background.

3.2 *Autofluorescence in Living Cells/ex vivo Tissues*

To investigate the molecular origin of cellular autofluorescence in living cells/*ex vivo* tissues, multiphoton fluorescence lifetime imaging measurements were carried out on living cells maintained in culture media at room temperature. Three mammalian cell lines were used: (1) HEK 293T epithelial cell line, (2) primary hepatocyte cultures, and (3) HeLa cancer cells. Figure 5(a) shows the representative lifetime images obtained by exciting the specimens at 790 nm. Similar measurements were performed at multiple excitation wavelengths and the accompanying lifetime histogram [Fig. 5(b)] shows the lifetime distributions obtained by exciting the specimens

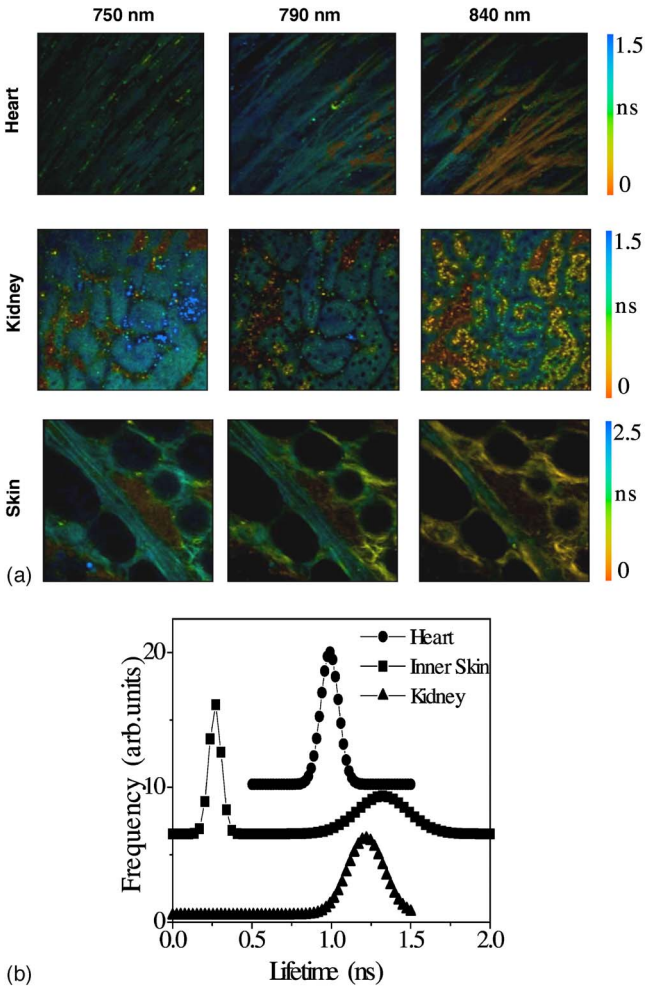

Fig. 6 Representative lifetime images obtained from mouse tissues for (a) transmission, multiphoton intensity, and multiphoton lifetime images obtained from heart, kidney, and skin of a mouse. Specimens were excited at three excitation wavelengths; 750, 790, and 840 nm. (b) Representative lifetime histogram (at 790-nm excitation) showing single component lifetime analysis in these tissues, demonstrating clear lifetime contrast in tissues with varying metabolic activity. Baselines for histograms of skin and heart are shifted in the *y* axis (arbitrary scale) for the sake of clarity.

at three representative wavelengths. It was observed that each cell line has its own characteristic lifetime signatures of autofluorescence. Figure 6 shows the lifetime images and histograms obtained from three freshly excised *ex vivo* tissues from a 20-month-old female mouse. All these images were obtained by exciting the specimens at 790 nm and by collecting fluorescence emission with a short pass filter (SP 640 nm). One can clearly see that there are obvious structural differences in different tissues that are accompanied by distinct lifetime signatures. Besides these structural differences, the autofluorescence intensities for all these tissues were similar in magnitude.

3.3 *Molecular Origins of Autofluorescence in Cells/Tissues*

The major molecular players in governing the cellular autofluorescence are the reduced nicotinamide adenine dinucleotide (NADH) and the flavoproteins.[22,23] Minor contributions from elastin and collagen are also reported.[24] Table 1 shows the common autofluorescence molecules and their typical absorption/emission maxima with single photon excitation. Historically, the endogenous autofluorescence of cells was used to monitor the metabolic state of living tissues. It is known that the ratio of oxidized and reduced electron carriers gives a measure of steady state cellular metabolism. A quantitative estimate of this redox ratio can be calculated by separating out the contributions from reduced pyridine nucleotides (NADH and NADPH) and oxidized flavoproteins (FP) in cells. There have been numerous reports in the past employing either spectroscopic methods or intensity-based imaging methods for estimating this ratio.[1,2] As one can envisage, the reliability in estimating the redox ratio based on spectroscopic/intensity variations is greatly affected by the artifacts, which include absorption and scattering of the excitation light as well as due to spatial variation of concentration of metabolic cofactors/enzymes in the cell. Lifetime measurements are relatively insensitive to these artifacts and therefore can provide a reliable estimate of metabolic processes in living cells. Lifetime histograms in Fig. 5(b) were obtained by assuming a single exponential decay model in the analysis of lifetime images. Although multiexponential decays were observed in all the cells studied, this monoexponential approximation illustrates a few intriguing features: first, normal cell lines (primary hepatocyte cultures and HEK293T epithelial cell line) have relatively higher lifetime than the cancer cell lines (HeLa), irrespective of the excitation wavelength used. Second, the mean lifetime values calculated with different excitation wavelengths vary with different excitation wavelengths, suggesting that multiple lifetime contributions with varying amplitudes are present in different cell lines. Finally, the lifetime images are independent of wide variation in concentration that was observed across the cell. A preliminary analysis of multicomponent lifetime was carried out to estimate the different contributions and is summarized in Table 2. Two major lifetime contributions were found in all the cells: (1) $\tau_1 \sim 0.48 \pm 0.1$ ns and (2) $\tau_2 \sim 2.4 \pm 0.3$ ns. The relative amplitudes of these contributions vary among the different cell lines investigated. The short lifetime component $\tau_1 \sim 0.48$ ns corresponds to free NADH and closely resembles that observed in other studies as well as to that observed for β-NADH solution in our own experiments (data not shown). Earlier studies in NADH solutions with binding proteins have

Table 1 Common sources of autoflourescence in cells/tissues.

Fluorophore	Absorption Maximum (nm)	Emission Maximum (nm)
Tryptophan	280	348
Collagen	275	300
Elastin	300–340	420–460
NADH	340	420–460
NAD(P)H	370	470
Flavins	480	500–550

Table 2 Two-component lifetime analysis of cellular autofluorescence.

	750 nm				790 nm			
Cells	τ_1 (ns)	A_1 (%)	τ_2 (ns)	A_2 (%)	τ_1 (ns)	A_1 (%)	τ_2 (ns)	A_2 (%)
HEK 293T	0.50±0.1	68	2.4±0.3	32	0.50±0.1	62	2.4±0.3	38
Hepatocytes	0.45±0.1	50	2.3±0.3	50	0.45±0.1	46	2.3±0.3	54
HeLa	0.48±0.1	80	2.5±0.3	20	0.48±0.1	72	2.5±0.2	28

reported[25,26] a longer lifetime value for protein-bound NADH with a mean lifetime of 2.0 to 2.4 ns, and this corresponds to the second component of lifetime observed in our measurements. A recent multiphoton absorption study in NAD(P)H and flavoproteins by Huang et al.[23] reported that at 750-nm excitation, only NADH gets effectively excited, whereas flavoprotein fluorescence contributions become appreciable only for excitation wavelengths >790 nm. In accordance with these findings, we can anticipate that only NAD(P)H gets excited at 750 nm, whereas flavoproteins are the main contributors for excitation wavelengths >790 nm. Contributions from both NAD(P)H and flavoproteins are detected for wavelengths >790 nm. At 790- and 830-nm excitations, a third lifetime component with a wider distribution and smaller amplitude (~15%) was observed with $\tau_3 \sim 3.2 \pm 0.5$ ns in all the cell lines. It may be attributed to oxidized flavoproteins, as observed in some of the earlier spectroscopic studies and reported to have mean lifetime values of 3 to 5 ns in their free state and ~1 ns in the protein-bound state.[23,27] Although this third component was qualitatively found in all the cells for excitation wavelengths larger than 790 nm, we found that detected photon counts in our measurements were not sufficient to enable quantitative interpretation of this third component reliably. We would therefore limit our further discussion only to a two-component analysis without overstating the importance of the minor third lifetime component in cells/tissues. As can be seen from both Fig. 5 and Table 2, normal cells have larger contributions from free flavoproteins and protein-bound NADH, whereas the cancer cells have predominantly contributions free NAD(P)H and possibly protein-bound flavoproteins. It has been recently shown that metabolic rate of tumor tissue can be correlated with a higher ratio of reduced pyridine nucleotides to oxidized flavoproteins.[28] Unlike these earlier studies, which relied on spectroscopic redox ratio, our results demonstrate a method to obtain a direct estimate of redox ratio spatially resolved in cells based on intrinsic lifetime parameter and with a single excitation wavelength (790 nm). We calculated the redox ratio from the amplitudes of two lifetime components given in Table 2 for the cell lines used in this study. Figure 5(c) shows qualitatively the differences in metabolic activity in these cell lines. This possibility is further substantiated in Fig. 6, where mouse tissues with different metabolic activities are distinguished based on their lifetime signatures. It is possible that minor lifetime contributions from collagen and elastin are also detected in this observation window. While this paper was under review, an interesting study by Blinova et al.[29] reported steady state kinetics of mitochondrial matrix NADH and the authors observed three distinct lifetime pools of NADH [0.4 (63%), 1.8 (30%), and 5.7 ns (7%)] in isolated mitochondria based on time-resovled single photon, spectroscopic measurements. Although these results are similar to our data, note that flavoprotein contributions cannot be neglected in interpreting cellular autofluorescence, and our analysis is more realistic in that regard.

3.4 *Photon Detection Efficiency, Photon Statistics, and Multicomponent Lifetime Analysis*

Cells in culture and turbid tissues can display complex, wavelength-dependent autofluorescence signatures that can have multiple molecular sources. Some of these signals have significantly overlapping emission spectra, which makes it a challenging task to isolate different autofluorescence signals reliably. Filter-based intensity methods can detect only a convolved, time-averaged signal from the different contributions. As demonstrated from the lifetime imaging histograms [Figs. 5(b) and 6(b)], although the emission spectral window was kept the same in all the measurements, characteristic lifetime differences were observed in different cell lines and in tissues. Any improvisation in the accuracy of the multicomponent lifetime analysis presented in Table 2 depends mainly on detector time resolution and photon statistics.

The photon detectors that are currently being used in lifetime imaging are the fast photomultiplier tubes (~150 to 300 ps) and microchannel plate (~50 to 100 ps). Streak camera detection improves the time resolution to ~2 to 15 ps. In the multigate detection approach, the lifetime is extracted by measuring the fluorescence signal in at least two different time-gated windows. It is known that the photon utilization and time resolution of the multigate detection approach are still limited by the detector performance.[11] One can also not avoid background noise arising from scattered fluorescence emission when an imaging (area) detector is used in multigate detection. Regardless of these limitations, the multigate detection FLIM methodology has been found to be very successful with single-photon excitation in the past. For multiphoton applications, it is imperative to use point-scanning detectors to eliminate background noise. Streak imaging essentially gives 4-D (intensity, time, x and y axes) information with high photon efficiency. In streak imaging, there is no "gating" of fluorescence emission so that the complete fluorescence decay curves can be collected and then used to extract lifetime information at individual pixels. The streak camera has good radiant sensitivity over a wide bandwidth of wavelengths, making it suitable for both single-photon and

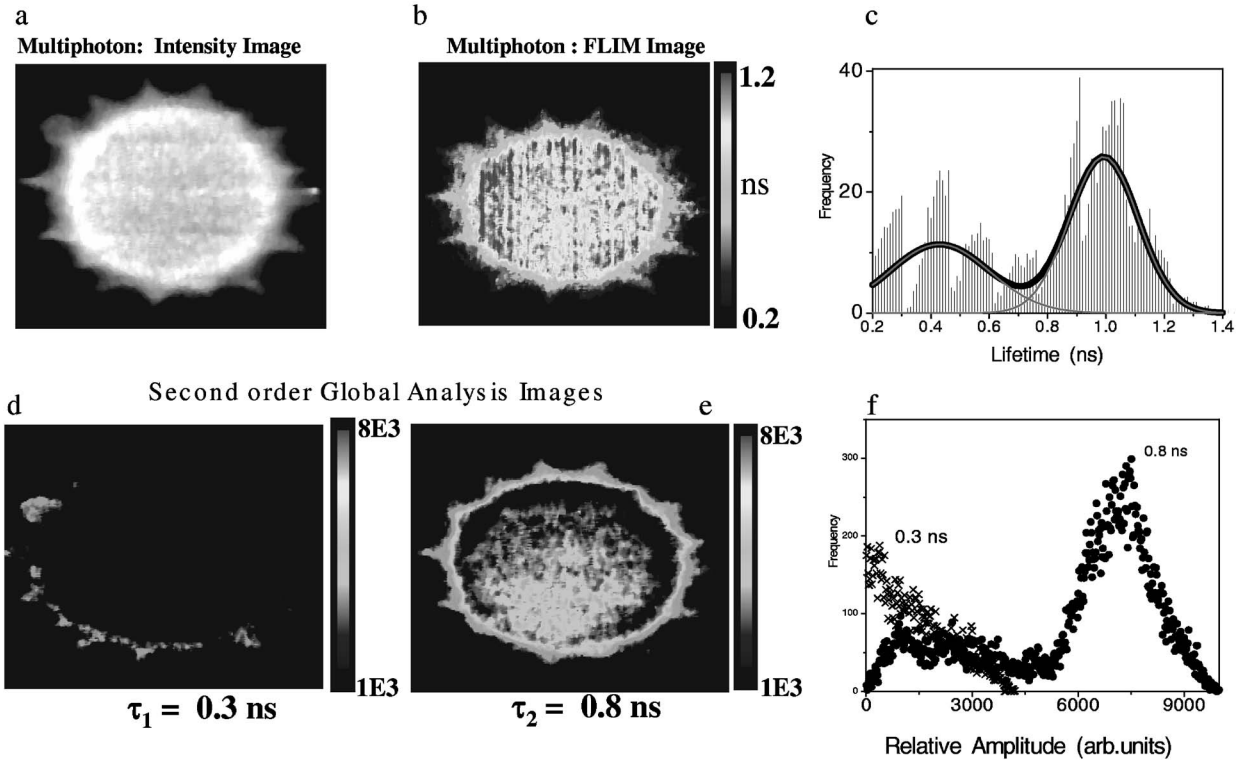

Fig. 7 Principle of global analysis for multicomponent lifetime analysis. A pollen grain specimen, stained with two different dyes, was excited at 840 nm. Lifetime images were obtained with the StreakFLIM system coupled to an Olympus IX-70 microscope. A single-component lifetime analysis (a) and (b) according to Eq. (1) shows two distinct peaks in the histogram (c). On the other hand, a second-order global analysis according to Eq. (2) shows two lifetime components, 0.3 and 0.8 ns, with varying amplitudes (d) and (e) across the field of view. (f) Lifetime histogram showing the relative amplitudes of the observed two components.

multiphoton imaging applications without compromising on detection sensitivity.[30] A more detailed exposition of this aspect will be published elsewhere.

In this section, we briefly describe two approaches for extracting multicomponent lifetimes in scanning microscopes. Traditionally, multicomponent lifetime analysis is performed by solving a time-dependent intensity function $F(x,y,t)$ at each pixel (x,y):

$$F(x,y,t) = A_1(x,y)\exp\left[\frac{-t}{\tau_1(x,y)}\right] + A_2(x,y)\exp\left[\frac{-t}{\tau_2(x,y)}\right], \quad (1)$$

where τ_1 and τ_2 are lifetime components with spatially varying amplitudes $A_1(x,y)$ and $A_2(x,y)$. The constants A_1, A_2, τ_1, and τ_2 are calculated at each pixel with an assumption that intensity decay at any position (x_1,y_1) is independent of decay at any other position (x_2,y_2). Although realistic, this assumption requires a very high photon count ($\sim$ two orders of magnitude more than for single-component analysis) at each pixel to achieve reasonable ($<5\%$) accuracy. In this context, an alternative approach may be adopted by assuming spatially invariant lifetime values for the two components as in the following equation:

$$F(x,y,t) = A_1(x,y)\exp\left(\frac{-t}{\tau_1^m}\right) + A_2(x,y)\exp\left(\frac{-t}{\tau_2^m}\right), \quad (2)$$

where τ_1^m and τ_2^m are the spatially invariant lifetimes of the two components. In this approximation (termed global analysis), the mean lifetime at any arbitrary pixel is governed by the varying amplitudes A_1 and A_2. In the global analysis approach, a better resolution of closed spaced parameters is achieved through simultaneous analysis of multiple sets of related data by assuming that some of the parameters are identical for each data set while the remaining parameters may differ. This approach has been found to yield statistically better results than the traditional two-component fitting in limited situations.[31] Figure 7 demonstrates the principle of global analysis in a pollen grain specimen with two lifetime components. In this example, the two lifetime components are assumed to be spatially invariant and the spatial variation of relative amplitudes [A_1 and A_2 in Eq. (2)] is shown. Note that different approximations in multicomponent lifetime analysis are applicable in limited situations and one must take care to validate the assumptions in each model in the biological situation before interpreting the results. For instance, assigning certain parameters to be invariant (i.e., globally shared between the data sets) invokes an *a priori* assumption of a physical model on the system. Several models should be tested in such a situation to verify the best model. Still, a good

fit itself cannot be regarded as proof of a model while fitting with exponentials. Ladokhin and White point out in this regard that physical relevance should be the chief criterion for accepting a model.[32] In situations where the lifetime of the fluorescent probe varies at various locations of the cell (e.g., spatially varying pH or energy transfer events), a global analysis approximation is less applicable and may have to be modified suitably. A realistic global fitting algorithm based on image segmentation developed by Pelet et al.[33] takes into account the correlation of fluorophore distribution with the morphology of cells/tissues. We are currently investigating extending the scope of this global analysis approach to resolve multiple autofluorescence contributions in unstained tissues.

4 Perspectives

The main aim of this paper is to demonstrate a quantitative method to investigate autofluorescence signatures in living cells and tissues by fluorescence lifetime imaging. Although the results presented in this paper are preliminary, they point out a novel possibility to determine the spatially resolved redox ratio responsible for cellular metabolism without any spectroscopic artifacts. An immediate consequence of this approach can be in monitoring *in vivo* modifications in tissue pathology by correlating the observed lifetime contributions to disease-specific changes in tissue fluorescence. The importance of probing endogenous fluorescence as compared to overexpressed fluorescent proteins or external fluorescent staining is the flexibility in observing the native cellular fluorescence and its modifications in various disease states. Recently, Troy et al. carried out a quantitative evaluation of the sensitivity of detection of fluorescent reporters in animal models and found that the signal-to-background ratio in fluorescence imaging is typically 8, which is lower than that in cells by a few orders of magnitude.[34] A key to successful disease diagnosis is to detect the onset of a disease at a very early stage. In the case of tumor diagnosis, for example, this implies the ability to detect a small number of fluorescent tumor cells amid the overwhelming autofluorescence background. From the preceding discussion of poor SNR, it can be understood that with intensity-based, wide-field imaging of tissues, it is impractical to detect a very small number of fluorescent cells within a growing tumor. A more quantitative approach is to employ optical sectioning methods such as confocal or multiphoton excitation microscopy to obtain information from different layers of the tissues. Although these methods offer better spatial resolution and deep tissue imaging possibilities, the autofluorescence background still poses problems in quantification. This is due to the fact that the photon detectors cannot discriminate the photons coming from the fluorescent tumor cells and autofluorescence background based on their intensity. Toward this direction, the results presented in this paper indicate that fluorescence lifetime imaging microscopy can be a valuable addition to the repertoire of autofluorescence imaging approaches currently available. Lifetime imaging can discriminate fluorescent proteins/dyes and autofluorescence based on their photophysical decay constants although their intensities are comparable, thereby providing a better contrast in deep tissue imaging. This approach becomes particularly advantageous when external staining is not desirable or is toxic to the tissues. This opens up a novel possibility to extend the sensitivity of the autofluorescence imaging by lifetime determinations to monitor pathological modifications (tumor progression, apoptosis) in small animals *in vivo*. Spectroscopic measurements reveal that autofluorescence intensity decreases in tumor tissues. Intensity reduction can also occur because of differential absorption or scattering factors in tissues. Reliability in interpreting for diagnostics should be ensured by a concentration-independent parameter and this further substantiates the importance of lifetime measurements in quantitative autofluorescence imaging. To maximize the utility of lifetime measurements in disease diagnosis, it will be worth implementing a hybrid modality that encompasses diffuse optical tomography and ultrasound measurements in addition to fluorescence lifetime imaging. This will be a powerful combination of complementary techniques in achieving 3-D information from the whole animal without compromising high spatial/temporal resolution. This aspect may open a new arena of molecular finger printing of cancer tissues. In situations where fluorescent molecules are used as tracers in tumor imaging, it will be useful to design novel NIR probes with longer lifetimes to achieve maximum lifetime discrimination from autofluorescence. Lifetime measurements can also reveal useful information regarding the *in vivo* pharmacokinetics of certain drugs such as photosensitizers in photodynamic therapy. Although lifetime measurements are gaining increasing recognition, they are still not cost effective, mainly because of the fact that the high-power pulsed lasers and fast photon detectors are expensive. It is anticipated that relatively inexpensive diode laser modules and detectors with good time resolutions may become available in the future, which might open a new direction for lifetime imaging to be implemented in routine clinical diagnosis and *in vivo* monitoring of therapy.

Acknowledgments

We gratefully acknowledge Kinton Armmer for helping with hepatocyte isolation and for tissue specimens and Pamela Larsen for *C. elegans* worms. Technical support from Takashi Ito (Hamamatsu Photonics, Japan) and Butch Moomaw (Hamamatsu Photonics, USA) are greatly appreciated.

References

1. R. Richards-Kortum and E. Sevick-Muraca, "Quantitative optical spectroscopy for tissue diagnosis," *Annu. Rev. Phys. Chem.* **47**, 555–606 (1996).
2. S. Andersson-Engels, C. Klinteberg, K. Svanberg, and S. Svanberg, "In vivo fluorescence imaging for tissue diagnostics," *Phys. Med. Biol.* **42**, 815–824 (1997).
3. E. Regar, J. A. Schaar, E. Mont, R. Virmani, and P. W. Serruys, "Optical coherence tomography," *Cardiovasc. Radiat. Med.* **4**, 198–204 (2003).
4. C. H. Tung, U. Mahmood, S. Bredow, and R. Weissleder, "In vivo imaging of proteolytic enzyme activity using a novel molecular reporter," *Cancer Res.* **60**(17), 4953–4958 (2000).
5. B. W. Pogue, C. Willscher, T. O. McBride, U. L. Osterberg, and K. D. Paulsen, "Contrast-detail analysis for detection and characterization with near-infrared diffuse tomography," *Med. Phys.* **27**, 2693–2700 (2000).
6. A. Periasamy, Eds., *Methods in Cellular Imaging*, Oxford University Press, New York (2001).
7. J. B. Pawley, Ed., *Handbook of Biological Confocal Microscopy*, Plenum Press, New York (1995).
8. K. Konig, "Multiphoton microscopy in life sciences," *J. Microsc.* **200**, 83–104 (2000).
9. E. Gratton, S. Breusegem, J. Sutin, Q. Ruan, and N. Barry, "Fluorescence lifetime imaging for the two photon microscope: time-domain

and frequency-domain methods," *J. Biomed. Opt.* **8**, 381–390 (2003).
10. J. Sytsma, J. M. Vroom, C. J. de Grauw, and H. C. Gerritsen, "Time-gated lifetime imaging and micro-volume spectroscopy using two-photon excitation," *J. Microsc.* **191**, 39–51 (1998).
11. H. C. Gerritsen, M. A. H. Asselbergs, A. V. Agronskaia, and W. G. J. A. H. M. Van Sark, "Fluorescence lifetime imaging in scanning microscopes: acquisition speed, photon economy and lifetime resolution," *J. Microsc.* **206**, 218–224 (2002).
12. W. Becker, A. Bergmann, M. A. Hink, K. König, and C. Biskup, "Fluorescence lifetime imaging by time-correlated single-photon counting," *Microsc. Res. Tech.* **63**, 58–66 (2004).
13. A. Schonle, M. Glatz, and S. W. Hell, "Four-dimensional multiphoton microscopy with time-correlated single-photon counting," *Appl. Opt.* **39**, 6308–6311 (2000).
14. W. Becker, A. Bergmann, and G. Weiss, "Lifetime imaging with the Zeiss LSM-510," *Proc. SPIE* **4620**, 30–35 (2002).
15. R. V. Krishnan, H. Saitoh, H. Terada, V. E. Centonze, and B. Herman, "Development of a multiphoton fluorescence lifetime imaging microscopy (FLIM) system using a streak camera," *Rev. Sci. Instrum.* **74**, 2714–2721 (2003).
16. R. V. Krishnan, J. Zhang, E. Biener, R. Heckel, and B. Herman, "Probing subtle fluorescence dynamics in cellular proteins by streak camera based fluorescence lifetime imaging microscopy," *Appl. Phys. Lett.* **83**, 4658–4660 (2003).
17. *Guide to Streak Cameras*, Hamamatsu Photonics, Hamamatsu City, Japan (1996).
18. Y. Zhang, E. Chong, and B. Herman, "Age-associated increases in the activity of multiple caspases in Fisher 344 rat organs," *Exp. Gerontol.* **37**, 777–789 (2002).
19. J. Zhang, R. E. Campbell, A. Y. Ting, and R. Y. Tsien, "Creating new fluorescent probes for cell biology," *Nat. Rev. Mol. Cell Biol.* **3**, 906–918 (2002).
20. P. van Roessel and A. H. Brand, "Imaging into the future: visualizing gene expression and protein interactions with fluorescent proteins," *Nat. Cell Biol.* **4**, E15–20 (2002).
21. R. M. Hoffman, "Green fluorescent protein imaging of tumour growth, metastasis and angiogenesis in mouse models," *Lancet Oncol.* **3**, 546–556 (2002).
22. J. V. Rocheleau, W. S. Head, and D. W. Piston, "Quantitative NAD(P)H/flavoprotein autofluorescence imaging reveals metabolic mechanisms of pancreatic islet pyruvate response," *J. Biol. Chem.* **279**, 31780–31787 (2004).
23. S. Huang, A. A. Heikal, and W. W. Webb, "Two-photon fluorescence spectroscopy and microscopy of NAD(P)H and flavoprotein," *Biophys. J.* **82**, 2811–2825 (2002).
24. M. J. Cole, J. Siegel, S. E. D. Webb, R. Jones, K. Dowling, M. J. Dayel, D. Parsons-Karavassilis, P. M. W. French, M. J. Lever, L. O. D. Sucharov, M. A. A. Neil, R. Juskaitis, and T. Wilson, "Time-domain whole field fluorescence lifetime imaging with optical sectioning," *J. Microsc.* **203**, 246–257 (2001).
25. K. Konig and I. Riemann, "High resolution multiphoton tomography of human skin with subcellular spatial resolution and picosecond time resolution," *J. Biomed. Opt.* **8**, 432–439 (2003).
26. R. Niesner, B. Peker, P. Schulusche, and K. H. Gericke, "Non-iterative biexponential fluorescence lifetime imaging in the investigation of cellular metabolism by means of NAD(P)H autofluorescence," *ChemPhysChem* **5**, 1141–1149 (2004).
27. J. R. Lakowicz, H. Szmachinski, K. Nowaczyk, and M. L. Johnson, "Fluorescence lifetime imaging of free and protein-bound NADH," *Proc. Natl. Acad. Sci. U.S.A.* **89**, 1271–1275 (1992).
28. Z. Zhang, H. Li, Q. Liu, L. Zhou, M. Zhang, Q. Luo, J. Glickson, B. Chance, and G. Zheng, "Metabolic imaging of tumors using intrinsic and extrinsic fluorescent markers," *Biosens. Bioelectron.* **20**, 643–650 (2004).
29. K. Blinova, S. Carroll, S. Bose, A. V. Smirnov, J. J. Harvey, J. R. Knutson, and R. S. Balaban, "Distribution of mitochondrial NADH fluorescence lifetimes: steady-state kinetics of matrix NADH interactions," *Biochemistry* **44**, 2585–2594 (2005).
30. R. V. Krishnan, J. Zhang, V. E. Cenonze, and B. Herman, "Streak FLIM: a novel technology for quantitative FRET imaging," Chap. 12 in *Methods in Cellular Imaging*, A. Periasamy and R. N. Day, Eds., Oxford University Press, New York (2005).
31. P. J. Verveer, A. Squire, and P. I. Bastiaens, "Global analysis of fluorescence lifetime imaging microscopy data," *Biophys. J.* **78**, 2127–2137 (2000).
32. A. S. Ladokhin and S. H. White, "Alphas and Taus of tryptophan fluorescence in membranes," *Biophys. J.* **81**, 1825–1827 (2001).
33. S. Pelet, M. J. R. Previte, L. J. Laiho, and P. T. C. So, "A fast global fitting algorithm for fluorescence lifetime imaging microscopy based on image segmentation," *Biophys. J.* **87**, 2807–2817 (2004).
34. T. Troy, D. Jekic-McMullen, L. Sambucetti, and B. Rice, "Quantitative comparison of the sensitivity of detection of fluorescent and bioluminescent reporters in animal models," *Molecular Imaging* **3**, 9–23 (2004).